



THE UNIVERSITY *of* EDINBURGH

## Edinburgh Research Explorer

### Searching for the Optimal Fluorophore to Label Antimicrobial Peptides

**Citation for published version:**

Zhao, C, Fernandez Vargas, A, Avlonitis, N, Vande Velde, G, Bradley, M, Read, ND & Vendrell, M 2016, 'Searching for the Optimal Fluorophore to Label Antimicrobial Peptides', *ACS Combinatorial Science*.  
<https://doi.org/10.1021/acscombsci.6b00081>

**Digital Object Identifier (DOI):**

[10.1021/acscombsci.6b00081](https://doi.org/10.1021/acscombsci.6b00081)

**Link:**

[Link to publication record in Edinburgh Research Explorer](#)

**Document Version:**

Peer reviewed version

**Published In:**

ACS Combinatorial Science

**Publisher Rights Statement:**

Author's final peer reviewed manuscript as accepted for publication.

**General rights**

Copyright for the publications made accessible via the Edinburgh Research Explorer is retained by the author(s) and / or other copyright owners and it is a condition of accessing these publications that users recognise and abide by the legal requirements associated with these rights.

**Take down policy**

The University of Edinburgh has made every reasonable effort to ensure that Edinburgh Research Explorer content complies with UK legislation. If you believe that the public display of this file breaches copyright please contact [openaccess@ed.ac.uk](mailto:openaccess@ed.ac.uk) providing details, and we will remove access to the work immediately and investigate your claim.



# Searching for the optimal fluorophore to label antimicrobial peptides

Can Zhao,<sup>1</sup> Antonio Fernandez,<sup>2</sup> Nicolaos Avlonitis,<sup>3</sup> Greetje Vande Velde,<sup>4</sup> Mark Bradley,<sup>3</sup> Nick D. Read,<sup>1,\*</sup> Marc Vendrell<sup>2,\*</sup>

<sup>1</sup> Manchester Fungal Infection Group, Institute of Inflammation and Repair, University of Manchester. CTF Building, Grafton St., M13 9NT Manchester, United Kingdom.

<sup>2</sup> MRC Centre for Inflammation Research, The University of Edinburgh. 47 Little France Crescent, EH16 4TJ Edinburgh, United Kingdom.

<sup>3</sup> EaStCHEM School of Chemistry, The University of Edinburgh. West Mains Road, Edinburgh EH9 3FJ, United Kingdom.

<sup>4</sup> Biomedical MRI Unit/MoSAIC, Department of Imaging and Pathology, KU Leuven, Leuven, Belgium.

KEYWORDS: fluorescence, labeling, imaging, probes, fungi, infection.

## **Abstract**

With the advent of antimicrobial resistance, there is an urgent need for new strategies to treat infectious diseases. Antimicrobial peptides are considered as promising candidates, and therefore there is a need to understand their mechanism of action in order to exploit their therapeutic potential. To this end, fluorescent analogs are powerful tools to analyze their behavior and subcellular localization in cells and in vivo. However, the conjugation of fluorophores to antimicrobial peptides, especially in short sequences, can impair their biological activity, making the selection of the fluorescent label an essential step in these studies. In the present work, we have systematically modified a model antifungal hexapeptide with a collection of fluorophores covering broad physicochemical and spectral properties. The resulting conjugates have been examined in two different fungal species, in terms of their activity and intracellular localization. The biological results confirm the influence of the different fluorescent moieties on the subcellular localization of antimicrobial sequences, and provides an insight on the optimal fluorophores to be used in the preparation of fluorescent peptides for different bioimaging assays.

## Introduction

In the past decades, fluorescent dyes have been broadly used as tags to visualize and study the roles of peptides in cells and in vivo.<sup>1</sup> For these studies, live cell imaging has become the technology of choice as it provides a direct readout of the localization of the peptides with high spatial and temporal resolution. In the context of antimicrobial peptides, several reports have described fluorescence labeling as an approach to study their mechanism of action<sup>2-4</sup> as well as to develop imaging probes for the rapid identification of microbes at infection sites.<sup>5</sup> In all cases, it is often assumed that fluorescently labeled peptides faithfully mimic the spatio-temporal dynamics of the native peptides, and fluorescent labels are typically chosen on the basis of excitation/emission wavelength, quantum yield, photobleaching, environmental sensitivity or chemical conjugation. Little attention has been paid to whether the fluorescent label might alter the physicochemical properties of the conjugate, and it is often unclear whether the fluorescent tag influences the uptake and localization of antimicrobial peptides inside living cells. In order to evaluate the impact that different fluorophores have in the biological properties of antimicrobial peptides and their application as imaging probes, we have synthesized a library of fluorescent conjugates based on the Peptide Antifungal 26 (PAF26).<sup>6</sup> This rationally designed hexapeptide exhibits high potency against filamentous fungi (including human and crop pathogens), low toxicity against bacterial cells and negligible toxicity against mammalian cells. PAF26 is currently being used as a model peptide for the characterization of the mode-of-action of small, cationic, cell penetrating antifungal peptides and for the design and development of synthetic antifungal peptides with improved properties for therapeutic uses.<sup>7</sup>

In the present work, we have conjugated 12 different fluorophores (either in-house or commercially available) to the peptide sequence of PAF26 and compared their biological activity, cellular uptake and intracellular localization using confocal live cell imaging. From these studies, we have observed that the activity of the conjugates is practically unaffected by the fluorescent labels whereas they accumulate in different intracellular regions depending on the fluorophore attached to the sequence. This systematic study will aid chemists working on peptide-based imaging agents in the selection of the fluorophores for different fluorescence-based biological applications.

## **Results and Discussion**

### **Design and synthesis of a library of fluorescent antifungal peptides**

For many years, the synthesis of antimicrobial peptides has been adapted to combinatorial chemistry. However, libraries of antimicrobial peptides have been mainly focused on the optimization of the peptide sequences, either to enhance their antimicrobial activity, improve their selectivity against specific strains or pathogens, or to reduce their cytotoxicity in mammalian cells.<sup>8-10</sup> Some antimicrobial peptides have been labeled with fluorophores in order to visualize their localization in cells by confocal microscopy.<sup>4,11</sup> More recently, the high selectivity of antimicrobial sequences has been exploited to develop imaging contrast agents for the rapid identification of infection sites.<sup>12,13</sup> In most reports, only one fluorophore is employed on the basis of its compatibility with the experimental procedures. However, conventional fluorophores differ largely in their physicochemical features,<sup>14,15</sup> and therefore it is reasonable to expect that different fluorophores could induce variability in the activity and cellular localization properties of peptide sequences. For instance, Baker et al. reported the influence of different fluorescent labels in a

combinatorial library of A<sub>1</sub>R adenosine inhibitors, where significant differences were observed in the binding properties of several fluorescently-labeled inhibitors.<sup>16</sup> In the context of short antimicrobial peptides, there are no reports of any systematic evaluation of their biological properties after conjugation to various fluorescent labels. Herein, we have designed a library based on the antimicrobial peptide sequence PAF26, which was modified with a total of 12 fluorophores covering the whole spectral range (from blue to near-infrared emission) and diverse physicochemical properties (Chart 1). In addition to conventional fluorophores (e.g. carboxyfluorescein, carboxyrhodamine, BODIPY, cyanine), we also included small fluorophores (e.g. NBD, dansyl), compounds with environmentally-sensitive properties (e.g. Nile Blue, malachite green, styryl), pH-sensitivity (e.g. naphthalimide) and esterase-activatable fluorophores (e.g. fluorescein diacetate). Overall, these fluorophores constitute a representative collection of the fluorescent labels that most chemists would employ for labeling any defined peptide sequence.

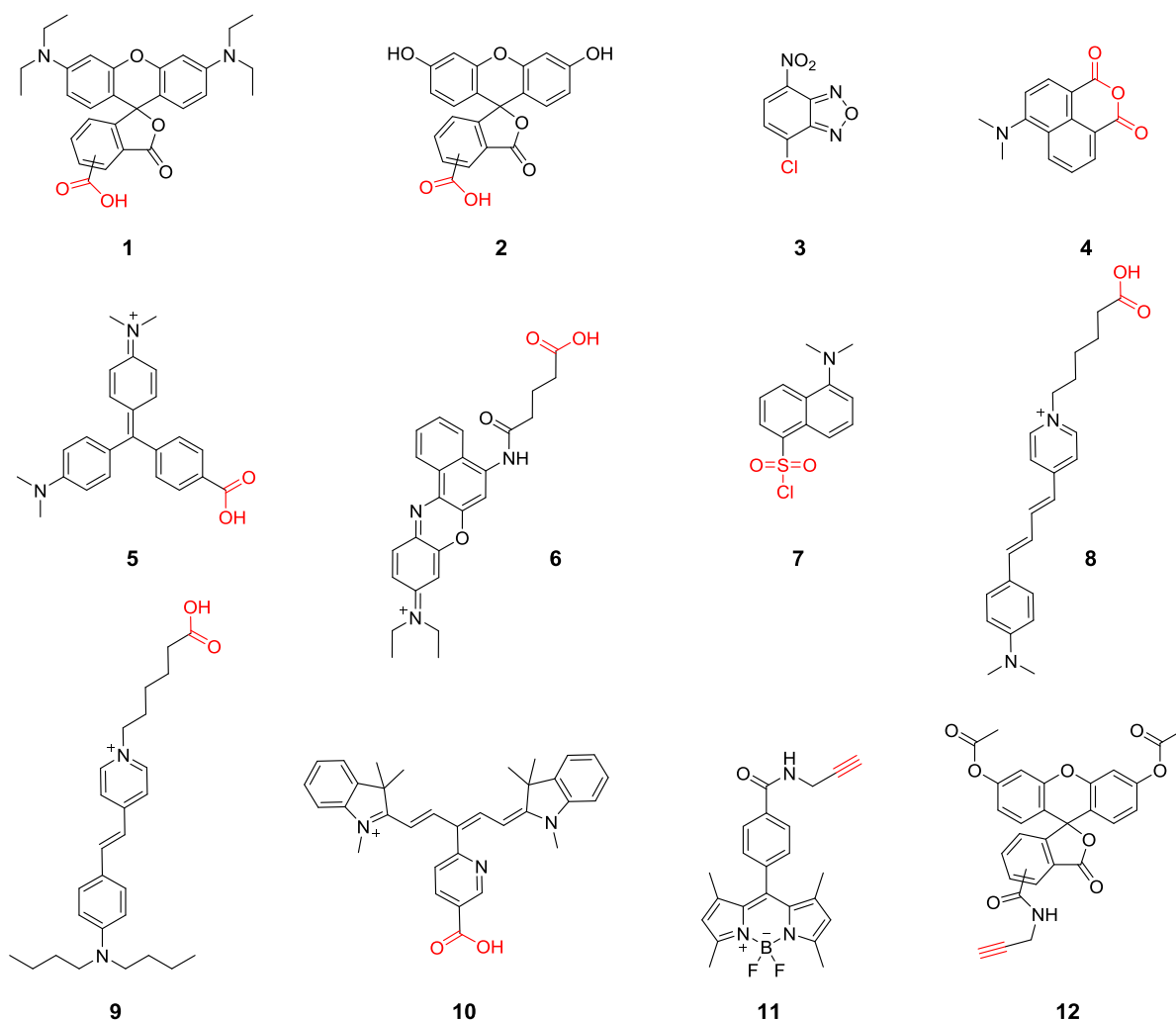
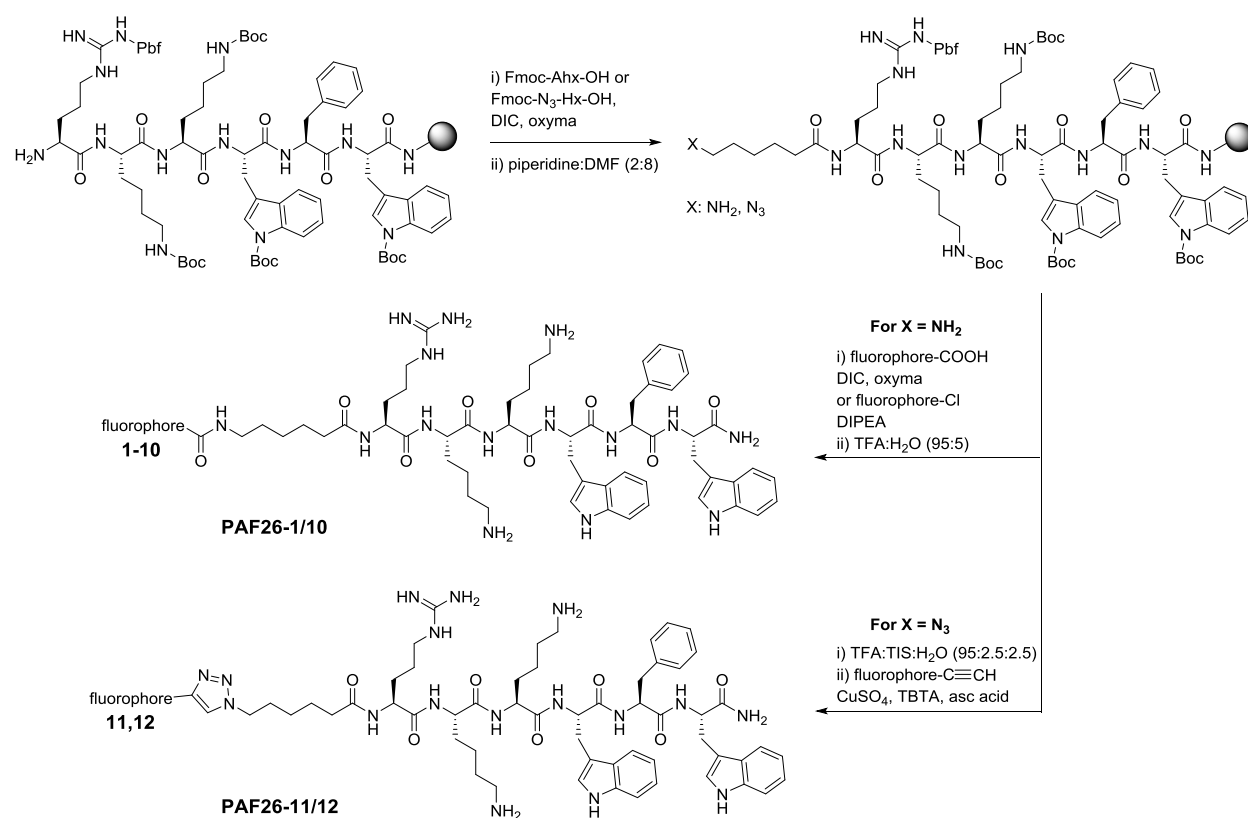


**Chart 1. Fluorescent labels for the derivatization of the antimicrobial peptide PAF26.** We employed 12 different fluorophores with suitable reactive groups (in red) for peptide labeling (e.g. carboxylic acids, sulfonyl chlorides, anhydrides, alkynes). Fluorophores **1**, **2**, **3** and **7** are commercially available, whereas the synthesis and characterization of all other fluorophores is described in the Experimental Procedures and the Electronic Supplementary Information (ESI).

PAF26 (H-RKKFW-NH<sub>2</sub>) is a short antimicrobial peptide which, like many other antimicrobial peptides, contains both cationic and hydrophobic residues,<sup>6,7</sup> and therefore it is an excellent model for examining the influence of fluorophores in the properties of antimicrobial peptides. We

designed the synthesis of the hexapeptide using conventional solid-phase protocols in Rink amide polystyrene resin (Scheme 1). In order to incorporate suitable conjugation groups within the sequence of PAF26, we first synthesized two derivatives containing aminohexanoic or azidohexanoic spacers directly attached to the *N*-terminal group of PAF26. Through these spacers, fluorophores could be readily conjugated using their reactive groups (i.e., carboxylic acids, chlorides, anhydrides, sulfonyl chlorides or alkynes) without affecting the main recognition features of the antimicrobial peptide. Most library members were fully synthesized on solid support, including the coupling of the fluorophore, to render the final fluorescent PAF26 analogues upon acidic cleavage from the resin using reported procedures.<sup>17</sup> Due to the lability of the fluorophores **11** and **12** (i.e., BODIPY and fluorescein diacetate, respectively) to acidic media, the corresponding derivatives **PAF26-11** and **PAF26-12** were prepared by 1,3-Huisgen dipolar cycloaddition using the azido-modified PAF26 and the fluorescent alkynes in solution phase (Scheme 1). All 12 fluorescent derivatives of PAF26 were purified by semi-preparative HPLC to isolate the final conjugates (**PAF26-1** to **PAF26-12**) in high purities (for characterization data, see ESI).





**Scheme 1. Solid-phase synthesis of a library of fluorescent antimicrobial peptides based on the hexapeptide PAF26.** The peptide sequence of PAF26 was modified with amino- or azidohexanoic spacers at the *N*-terminus to enable the conjugation of different fluorophores, either by formation of amide bonds in solid-phase or by ‘click’ chemistry in solution. All 12 conjugates **PAF26-1** to **PAF26-12** were isolated in good yields and high purities. For the chemical structures of the fluorophores **1-12**, see Chart 1.

### In vitro biological activity of fluorescent antifungal peptides

After completing the synthesis of the library of fluorescent antimicrobial conjugates (**PAF26-1** to **PAF26-12**), we measured their spectral properties and determined their IC<sub>50</sub> values in two different fungal species (i.e., *Neurospora crassa* and *Aspergillus fumigatus*) as a measure of their cellular activity (Table 1). *N. crassa* has been widely used as an experimental model organism for filamentous fungi.<sup>18</sup> *A. fumigatus* is a very important opportunistic pathogen responsible for

multiple human diseases, the most lethal of which, invasive pulmonary aspergillosis, causes around 200,000 deaths per year.<sup>19</sup>

Conjugates incorporating small fluorophores (e.g., NBD (**PAF26-3**), naphthalimide (**PAF26-4**), dansyl (**PAF26-7**)) showed very similar antifungal activity when compared to the unlabeled sequence PAF26 in both fungal species. This observation is in line with previous reports where NBD or dansyl have been described as highly tolerated fluorescence labels for the derivatization of biomolecules.<sup>20</sup> Larger fluorophores, including positively-charged fluorophores [i.e. rhodamine (**PAF26-1**), Nile Blue (**PAF26-6**), styryl dyes (**PAF26-8** and **PAF26-9**)] and fluorescein-based structures (**PAF26-2** and **PAF26-12**) induced only minor differences in the antifungal activity of PAF26, with all IC<sub>50</sub> values in the low micromolar range. Two conjugates (**PAF26-10** and **PAF26-11**) showed slightly higher activity, being the two corresponding fluorophores [i.e. cyanine (**10**) and BODIPY (**11**)] permeable structures that have been reported for the preparation of a range of fluorescent probes.<sup>21-25</sup> Altogether, these results corroborate the minor influence of the fluorescence labels on the antifungal activity of fluorescent PAF26 conjugates, with the smallest impairment being observed for conjugates including small fluorophores.

**Table 1.** Spectral properties and antifungal activities of the fluorescent antimicrobial sequences.

| Compound              | $\lambda_{\text{exc.}}$ (nm) | $\lambda_{\text{em.}}$ (nm) | MW     | IC <sub>50</sub> ( <i>N. crassa</i> <sup>‡</sup> ) | IC <sub>50</sub> ( <i>A. fumigatus</i> <sup>‡</sup> ) |
|-----------------------|------------------------------|-----------------------------|--------|--|---|
| PAF26                 | n.d.                         | n.d.                        | 949.6  | 4.0 ± 0.7  | 8.0 ± 0.3   |
| PAF26-1 <sup>¥</sup>  | 563                          | 593                         | 1530.8 | 3.8 ± 0.1  | 6.9 ± 0.2   |
| PAF26-2 <sup>¥</sup>  | 498                          | 529                         | 1419.7 | 5.3 ± 0.2  | 9.1 ± 0.3   |
| PAF26-3               | 488                          | 552                         | 1225.6 | 4.4 ± 0.3  | 7.9 ± 0.1   |
| PAF26-4               | 450                          | 532                         | 1285.7 | 4.2 ± 0.2  | 8.0 ± 0.2   |
| PAF26-5               | 635                          | n.d.                        | 1416.8 | 4.1 ± 0.4  | 9.7 ± 0.5   |
| PAF26-6               | 635                          | 679                         | 1476.8 | 3.2 ± 0.2  | 5.8 ± 0.2   |
| PAF26-7               | 300                          | 350                         | 1295.7 | 4.0 ± 0.1  | 7.9 ± 0.2   |
| PAF26-8               | 465                          | 706                         | 1408.8 | 3.0 ± 0.1  | 7.7 ± 0.1   |
| PAF26-9               | 487                          | 621                         | 1466.9 | 2.6 ± 0.2  | 7.2 ± 0.4   |
| PAF26-10              | 633                          | 660                         | 1547.9 | 2.0 ± 0.1  | 4.2 ± 0.4   |
| PAF26-11              | 505                          | 540                         | 1494.8 | 2.2 ± 0.2  | 3.7 ± 0.2   |
| PAF26-12 <sup>¥</sup> | 503                          | 530                         | 1585.7 | 5.3 ± 0.2  | 9.9 ± 0.4   |

<sup>‡</sup> IC<sub>50</sub> values (μM) represented as means ± standard deviations (n=3).

<sup>¥</sup> Values obtained for the mixture of 5 and 6-carboxyisomers.

### Fluorescence confocal live cell imaging studies to analyze the localization of PAF26 conjugates in fungal cells

Next we performed live cell imaging experiments to examine the cellular uptake and intracellular localization of the different conjugates in *N. crassa* and *A. fumigatus* by confocal laser scanning microscopy. Concentrations in the low micromolar range were used, as these have been previously optimized for the non-passive uptake of PAF26.<sup>16</sup> As shown in Fig 1, the rhodamine **PAF26-1** derivative localized to the cell envelope (comprising the plasma membrane and the cell wall) and the intracellular vacuolar/vesicular system of *N. crassa* conidial germlings, The positive charge of

the rhodamine fluorophore might favour the interaction with the negatively charged phospholipids in the plasma membrane. In contrast, the carboxyfluorescein derivative **PAF26-2** showed a similar pattern of intracellular vacuolar distribution but reduced staining on the cell envelope (Fig. 1). The negative charge of carboxyfluorescein reduced the affinity of the conjugate for the cell envelope, with slower internalization (Table 1). Similarly, the diacetylated derivative (**PAF26-12**) showed preferential staining of the vacuolar lumens with no fluorescence detected in the plasma or intracellular membranes, because its fluorescence emission is triggered upon reaction with intracellular esterases (Fig. S1 in ESI). We performed co-localization experiments between **PAF26-12** and **PAF26-1** and observed that both conjugates displayed a similar pattern of cellular uptake, first appearing in small vesicles and then accumulating in larger cell vacuoles (Fig. S2 in ESI).

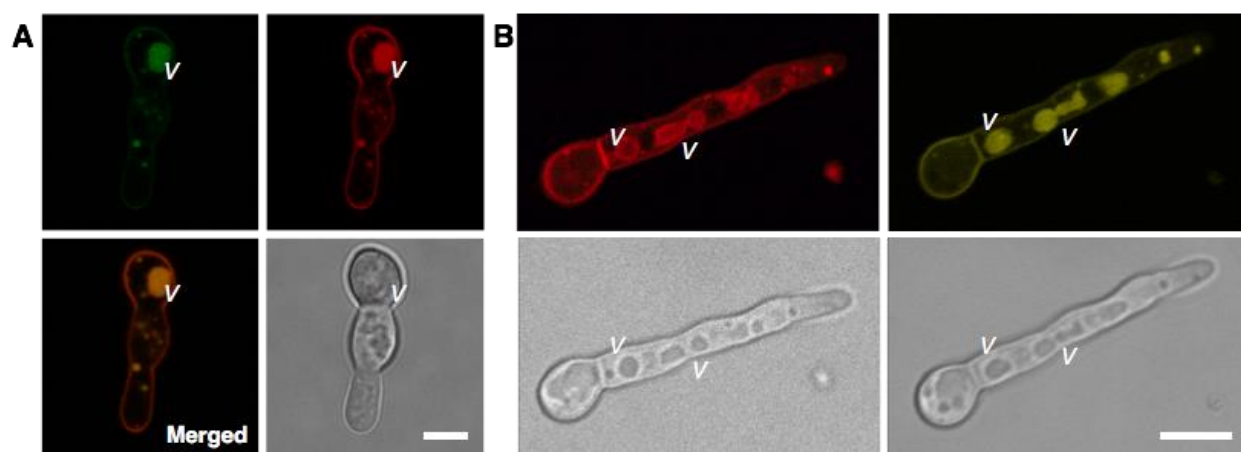


**Figure 1. Confocal fluorescence microscope images of conidial germlings of *N. crassa* after incubation with PAF26-1, PAF26-2 or PAF26-8.** A) Fluorescence images of *N. crassa* after co-staining with the rhodamine **PAF26-1** derivative (red, 0.5  $\mu$ M) and the carboxyfluorescein derivative **PAF26-2** (green, 0.5  $\mu$ M) at 25 °C. Scale bar: 2  $\mu$ m; v: vacuole. B) Imaging of *N. crassa* after co-staining with the styryl **PAF26-8** derivative (red, 1  $\mu$ M) and the rhodamine **PAF26-1** derivative (yellow, 1  $\mu$ M) at 25 °C. Scale bar: 5  $\mu$ m; v: vacuole.

Conjugates including small fluorophores, such as NBD (**PAF26-3**) or naphthalimide (**PAF26-4**), displayed similar intracellular vacuolar/vesicular localization, both in conidial germlings of *N. crassa* and *A. fumigatus* (Fig. S3 in ESI). Notably, the pH-sensitive properties of **PAF26-4** enabled preferential imaging of acidified vacuoles as opposed to the general vacuolar and vesicular structures staining observed with **PAF26-1** (Fig. S4 in ESI), demonstrating the possibility of monitoring intracellular pH changes in these subcellular structures. Conjugates including environmentally-sensitive fluorophores such as malachite green, Nile Blue or dansyl (**PAF26-5**, **PAF26-6** and **PAF26-7**) showed marginal staining in fungal cells, suggesting the potential accumulation of these peptide conjugates in neutral hydrophilic microenvironments (e.g. vacuoles), in which these fluorophores exhibit very low quantum yields.<sup>26,27</sup>

On the other hand, cationic styryl-based fluorophores (**PAF26-8** and **PAF26-9**) showed remarkably enhanced staining of the envelope of fungal cells. **PAF26-8** brightly stained the plasma and intracellular vacuolar/vesicular membranes of *N. crassa* to a similar extent than **PAF26-1** (Fig. 1), but without marked accumulation in the vacuole lumens. Imaging experiments using the **PAF26-9** derivative also showed a similar behavior in both *N. crassa* and *A. fumigatus* (Fig. S5 in ESI). As observed for **PAF26-1**, the cationic character of the styryl fluorophores favoured the rapid interaction with anionic components of the cellular membranes and enhanced their internalization (Table 1). Interestingly, and in contrast to the results obtained with *N. crassa* (Fig. 1), when we incubated **PAF26-8** with *A. fumigatus*, we did not observe the uptake of the fluorescent conjugate into healthy cells and hyphae were only stained once the cell membrane structure was compromised (Fig. S6 and Movie S1 in ESI). These results highlight differences in the internalization of **PAF26-8** by cells of different fungal species, suggesting the possibility of using fluorescent labels as means to improve the selectivity of antimicrobial sequences.

Finally, both cyanine and BODIPY-based conjugates (**PAF26-10** and **PAF26-11**, respectively) displayed a markedly different staining pattern when compared to all other members of the PAF26 library. The cyanine derivative (**PAF26-10**) brightly stained fungal cells and, besides localizing within vacuoles and vesicle lumens, it also stained other cytoplasmic organelles. Dual labeling experiments with the carboxyfluorescein derivative **PAF26-2** confirmed the presence of **PAF26-10** in the same vacuolar and vesicular organelles but also indicated its localization in different cytoplasmic organelles (Fig. 2). The BODIPY derivative **PAF26-11** exhibited general staining of the cytoplasm with no specific accumulation in subcellular organelles, as shown by co-localization experiments with **PAF26-1** (Fig. 2).

Furthermore, we compared the staining of *N. crassa* cells using the fluorescent peptides **PAF26-1**, **PAF26-2**, **PAF26-10** and **PAF26-11** and their corresponding fluorophores alone (Fig S7 in ESI). In these experiments, we observed that the PAF26 sequence is essential for the interaction, internalization and accumulation of the fluorescent conjugates in the vacuoles of fungal cells, as the fluorophores alone were not able to enter the cells or stained non-specifically intracellular environments (e.g. the BODIPY fluorophore showed bright, general staining of lipid-rich subcellular structures).

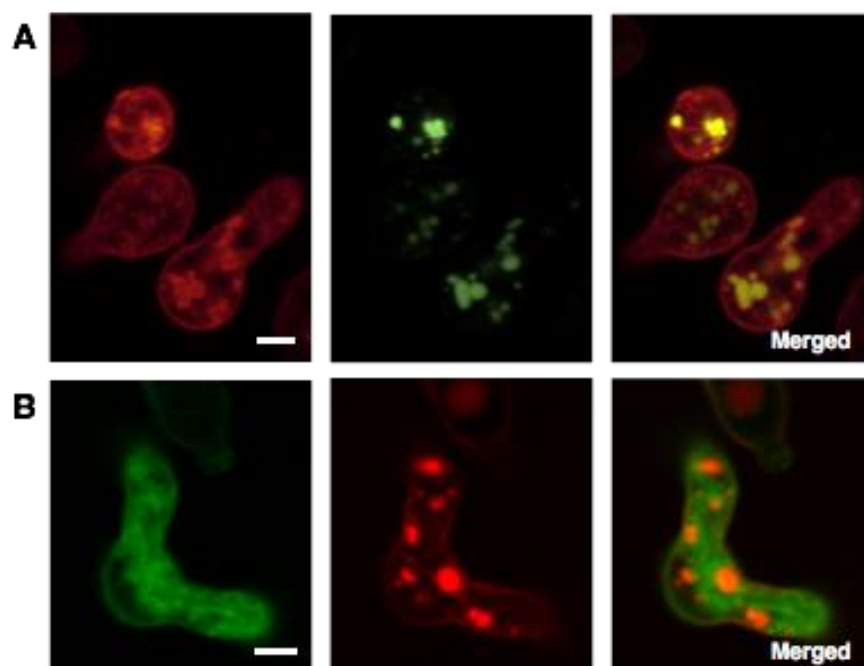


**Figure 2. Fluorescence microscope images of conidial germlings of *A. fumigatus* after incubation with PAF26-10 or PAF26-11.** A) Fluorescence images of *A. fumigatus* after co-staining with the cyanine **PAF26-10** (red, 1  $\mu$ M) and the carboxyfluorescein **PAF26-2** (green, 1  $\mu$ M) derivatives at 37 °C. Scale bar: 1  $\mu$ m. B) Fluorescence images of germinated *A. fumigatus* after co-staining with the BODIPY **PAF26-11** (green, 2  $\mu$ M) and the rhodamine **PAF26-1** (red, 2  $\mu$ M) derivatives at 37 °C. Scale bar: 1  $\mu$ m.

Finally, in view of the bright fluorescence signals in fungal cells upon incubation with **PAF26-10** (Figure 2A) and its emission in the near-infrared region ( $\lambda_{em.}$ : 660 nm, Table 1), we assessed the suitability of **PAF26-10** for whole-body in vivo fluorescence imaging experiments in mice with fungal lung infection. Near-infrared fluorophores are advantageous for in vivo imaging as the low autofluorescence background in such region of the spectra enhances the signal-to-noise ratios.<sup>28-30</sup> We determined the background and fluorescence signals in mice that had been treated with **PAF26-10**, and observed that the cyanine fluorophore was bright enough to provide a detectable

signal from live animals using whole-body fluorescence imaging (Fig. S8 in ESI). These results are in good agreement with previous reports of cyanine-labeled peptides for in vivo imaging of cancer cells in xenograft models.<sup>31,32</sup>

Altogether, the systematic evaluation of a library of fluorescent PAF26-based antimicrobial peptides provided important clues of the optimal fluorophores for the preparation of fluorescent peptides and their application in bioimaging experiments. Whereas positively-charged structures (e.g. rhodamine, styryl) favor the interaction with the anionic membrane components, neutral (e.g. NBD) and negatively-charged fluorophores (e.g. fluorescein) preferentially accumulate in vacuoles, and pH-sensitive fluorophores (e.g. naphthalimide) offer the possibility of visualizing specific intracellular processes in real time, such as vacuolar acidification. Cell permeable fluorophores (e.g. cyanine) provide bright cytosolic staining and show good discrimination from background signals in whole-body in vivo fluorescence imaging. These results suggest that, whereas the PAF26 sequence is the main component responsible for the antifungal activity of the fluorescent peptides, the incorporation of different fluorescent moieties into antimicrobial sequences can lead to major redistributions of the peptide sequences to different subcellular environments.

## **Conclusions**

Fluorescently labeled peptides are powerful tools for image-based mechanistic studies in cells. However, little is known about the influence of fluorescent tags in the uptake and localization of peptides inside the cells, and fluorophores are primarily selected on the basis of their spectral properties. We have evaluated the impact of different fluorophores (either commercially available or synthetically accessible) in the biological properties of a small model antimicrobial peptide by



synthesizing a library of fluorescent derivatives of the antifungal hexapeptide PAF26. Solid-phase peptide synthesis followed by conventional amide formation or solution-phase ‘click’ conjugation for acid-sensitive fluorophores rendered a collection of 12 fluorescent conjugates with broad spectral and physicochemical properties. The assessment of the fluorescent peptides in two fungal species (*N. crassa* and *A. fumigatus*) indicated the minimal impact of the fluorescent labels on the antimicrobial activity of the PAF26 sequence (with all conjugates displaying IC<sub>50</sub> values in the low micromolar range) whereas major changes in the localization pattern were observed upon conjugation to different fluorophores. This systematic study will aid chemists working on peptide-based imaging agents in the selection of optimal fluorophores for various fluorescence-based biological applications.

## Experimental Procedures

**8-(Dimethylamino)-3-oxatricyclo[trideca-1,5,7,9,11-pentaene]-2,4-dione (4).** 2.0 mL of dimethylamine aqueous solution (19.9 mmol) and a catalytic amount of CuSO<sub>4</sub> were added to a suspension of 4-bromo-1,8-naphthalenedicarboxylic anhydride (1.9 mmol) in DMF (50 mL). The mixture was then refluxed for 1.5 h, after which the solvent was evaporated under vacuum. Compound **4** was crystallized from ethanol as a yellow solid (275 mg, 57% yield). HPLC: *t<sub>R</sub>* = 4.74 min; MS (*m/z*): [M+H]<sup>+</sup> calcd for C<sub>14</sub>H<sub>11</sub>NO<sub>3</sub>: 242.1; found: 242.2; <sup>1</sup>H NMR (500 MHz, DMSO-*d*<sub>6</sub>): δ 8.59 (d, *J* = 8.4 Hz, 1H), 8.46 (d, *J* = 7.2 Hz, 1H), 8.32 (d, *J* = 8.4 Hz, 1H), 7.76 (t, *J* = 7.9 Hz, 1H), 7.20 (d, *J* = 8.4 Hz, 1H), 2.51 (s, 6H); <sup>13</sup>C NMR (126 MHz, DMSO-*d*<sub>6</sub>): δ 162.0, 160.8, 157.8, 134.8, 133.6, 133.0, 125.5, 124.1, 119.3, 113.2, 108.4, 44.7.

***N*-(4-((4-carboxyphenyl)(4-(dimethylamino)phenyl)methylene)cyclohexa-2,5-dien-1-ylidene)-*N*-methyldimethanaminium (5).** 4-(Bis(4-(dimethylamino)phenyl)methyl)benzoic acid (0.70 mmol) and *p*-chloranil (1.05 mmol) were dissolved in 30 mL CHCl<sub>3</sub>, and 0.5 mL AcOH was added to the solution. The solution was stirred for 1.5 h at 35°C. Compound **5** was crystallized in water to yield a green solid (176 mg, 70% yield). HPLC: *t<sub>R</sub>* = 4.28 min; MS (*m/z*): [M<sup>+</sup>] calcd for C<sub>24</sub>H<sub>25</sub>N<sub>2</sub>O<sub>2</sub><sup>+</sup>: 373.2; found: 373.2; <sup>1</sup>H NMR (500 MHz, DMSO-*d*<sub>6</sub>) δ 10.21 (s, 1H), 8.14 (d, *J* = 8.4 Hz, 2H), 7.46 (d, *J* = 8.4 Hz, 2H), 7.35 (d, *J* = 9.4 Hz, 2H), 7.11 (d, *J* = 9.5 Hz, 2H), 6.98 (d, *J* = 9.0 Hz, 2H), 6.64 (d, *J* = 9.0 Hz, 2H), 3.31 (s, 6H), 3.06 (s, 6H); <sup>13</sup>C NMR (126 MHz, DMSO-*d*<sub>6</sub>) δ 166.7, 157.0, 152.9, 151.6, 145.5, 144.6 (x 2), 140.5 (x 2), 132.7, 129.7, 128.9, 126.9 (x 2), 121.2 (x 2), 114.7 (x 2), 111.9 (x 2), 41.1 (x 2), 40.6 (x 2).

***N*-(5-(5-carboxybutanamido)-9*H*-benzo[*a*]phenoxazin-9-ylidene)-*N*-ethylethanaminium (6).** Nile Blue chloride (0.33 mmol) was dissolved in DCM together with glutaric anhydride (1 mmol) and DIPEA (1.14 mmol). The mixture was stirred at r.t. overnight. The crude mixture was then diluted with DCM and washed twice with water and then evaporated under vacuum. The crude

was then purified by column chromatography (DCM: MeOH, 9:1) to yield compound 6 as a dark blue solid (142 mg, 81% yield). HPLC:  $t_R$ : = 4.05 min; MS (m/z):  $[M^+]$  calculated for  $C_{25}H_{26}N_3O_4^+$ : 432.2; found: 432.2;  $^1H$  NMR (500 MHz, DMSO- $d_6$ )  $\delta$  8.75 (d,  $J$  = 8.0 Hz), 8.23 (s), 2.86 (q,  $J$  = 7.2 Hz), 2.35 (dt,  $J$  = 14.8 Hz, 4.6 Hz), 2.24 (t,  $J$  = 7.4 Hz), 1.93 – 1.77 (m), 1.71 (dd,  $J$  = 14.8 Hz, 7.4 Hz), 1.15 (d,  $J$  = 6.6 Hz);  $^{13}C$  NMR (126 MHz, DMSO- $d_6$ )  $\delta$  178.4, 174.6, 174.6, 164.2, 51.5, 33.3, 21.6, 21.3, 21.3, 20.5, 20.5, 19.1, 19.1, 18.9, 14.5, 14.5, 14.5, 12.3, 12.0.

**1-(5-carboxypentyl)-4-((1*E*,3*E*)-4-(4-(Dimethylamino)phenyl)buta-1,3-dienyl)pyridin-1-ium bromide (8).** 4-Methylpyridine (5.4 mmol) and ethyl 6-bromohexanoate (6.5 mmol) were dissolved in 20 mL of ACN, the mixture was refluxed at 90°C overnight. 1-(6-ethoxy-6-oxohexyl)-4-methylpyridinium was precipitated in cold Et<sub>2</sub>O:hexane (1:1) to yield a light brown solid (1.9 g, quantitative yield). HPLC:  $t_R$ : = 3.58 min; MS (m/z):  $[M^+]$  calcd for  $C_{14}H_{22}NO_2^+$ : 236.2; found: 236.2. 1-(6-ethoxy-6-oxohexyl)-4-methylpyridinium (1.6 mmol) and 3-(4-(dimethylamino)phenyl)acrylaldehyde (2 mmol) were dissolved in 10 mL of EtOH in a microwave reaction vessel, then pyrrolidine (1.6 mmol) was added to the solution. The mixture was irradiated under microwave for 10 min at 120 °C, and the crude was purified by column chromatography (DCM: MeOH, 9:1) to yield 4-((1*E*,3*E*)-4-(4-(dimethylamino)phenyl)buta-1,3-dien-1-yl)-1-(6-ethoxy-6-oxohexyl)pyridin-1-ium bromide as a red solid (853 mg, quantitative yield). The ethyl ester (0.25 mmol) was dissolved in 2 mL THF and 1 mL MeOH, mixed with LiOH (1.25 mmol) in water (1 mL) and stirred overnight at r.t. to yield the carboxylic acid which was used *in situ* without any further purification. Characterization data for the ester: HPLC:  $t_R$ : = 4.73 min; MS (m/z):  $[M^+]$  calcd for  $C_{25}H_{33}N_2O_2^+$ : 393.3; found: 393.4;  $^1H$  NMR (500 MHz, DMSO- $d_6$ )  $\delta$  8.80 (d,  $J$  = 6.9 Hz, 2H), 8.05 (d,  $J$  = 7.0 Hz, 2H), 7.87 – 7.77 (m, 2H), 7.48 (d,  $J$  = 8.9 Hz, 2H), 7.02 (d,  $J$  = 6.6 Hz, 2H), 6.78 – 6.71 (m, 2H), 4.05 (q,  $J$  = 7.1 Hz, 2H), 2.99 (s, 6H), 2.31 (td,  $J$  = 7.3,

2.1 Hz, 2H), 1.95 – 1.83 (m, 2H), 1.61 – 1.52 (m, 2H), 1.38 – 1.25 (m, 2H), 1.19 (t,  $J = 7.1$  Hz, 2H), 1.17 (t,  $J = 7.1$  Hz, 3H).  $^{13}\text{C}$  NMR (126 MHz, DMSO)  $\delta$  173.2, 153.6, 151.6, 144.1, 142.7, 129.6, 124.0, 123.6, 123.2, 112.5, 60.2, 59.5, 53.6, 33.6, 30.6, 25.3, 24.2, 23.0, 14.6.

**(*E*)-1-(5-carboxypentyl)-4-(4-(Dibutylamino)styryl)pyridin-1-ium bromide (9).** (*3E,5E*)-1-(6-ethoxy-6-oxohexyl)-4-methylpyridinium (1.6 mmol) and 4-(dibutylamino)benzaldehyde (2 mmol) were dissolved in 10 mL of EtOH in a microwave reaction vessel, then pyrrolidine (1.6 mmol) was added to the solution. The mixture was left to react under microwave irradiation for 10 min at 120°C. The crude was purified by column chromatography (DCM: MeOH, 9:1) to yield (*E*)-4-(4-(dibutylamino)styryl)-1-(6-ethoxy-6-oxohexyl)pyridin-1-ium bromide as a purple solid (703 mg, quantitative yield). The ethyl ester (0.25 mmol) was dissolved in 2 mL THF and 1 mL MeOH, mixed with LiOH (1.25 mmol) in water (1 mL) and stirred overnight at r.t. to yield the carboxylic acid which was used *in situ* without any further purification. Characterization data for the ester: HPLC:  $t_R = 5.76$  min; MS ( $m/z$ ):  $[\text{M}^+]$  calcd for  $\text{C}_{29}\text{H}_{43}\text{N}_2\text{O}_2^+$ : 451.3; found: 451.4.  $^1\text{H}$  NMR (500 MHz, DMSO- $d_6$ )  $\delta$  8.76 (d,  $J = 7.0$  Hz, 2H), 8.05 (d,  $J = 7.1$  Hz, 2H), 7.91 (d,  $J = 16.0$  Hz, 1H), 7.57 (d,  $J = 8.9$  Hz, 2H), 7.12 (d,  $J = 16.0$  Hz, 1H), 6.74 (d,  $J = 9.1$  Hz, 2H), 4.41 (t,  $J = 7.4$  Hz, 2H), 4.05 (q,  $J = 7.1$  Hz, 4H), 3.41 – 3.34 (m, 3H), 2.31 (td,  $J = 7.3, 1.6$  Hz, 2H), 1.98 – 1.84 (m, 2H), 1.63 – 1.47 (m, 4H), 1.41 – 1.25 (m, 4H), 1.20 (t,  $J = 7.1$  Hz, 3H), 1.17 (t,  $J = 7.1$  Hz, 3H), 0.93 (t,  $J = 7.4$  Hz, 6H).  $^{13}\text{C}$  NMR (126 MHz, DMSO)  $\delta$  173.2, 154.3, 150.4, 143.9, 142.8, 139.1, 131.0, 122.7, 122.2, 117.0, 112.0, 60.2, 59.3, 53.6, 50.3, 33.6, 30.6, 29.5, 25.3, 23.1, 20.1, 14.6.

**2-((1*E*,3*Z*)-3-(5-carboxypyridin-2-yl)-5-((*E*)-1,3,3-trimethylindolin-2-ylidene)penta-1,3-dien-1-yl)-1,3,3-trimethyl-3*H*-indol-1-ium iodide (10).** 3*H*-Indolium-2,3,3-tetramethyl iodide (0.72 mmol), NaOAc (0.72 mmol) and 6-(1,3-dioxopropan-2-yl) nicotinic acid (0.36 mmol) were

added to a microwave reaction vessel with 10 mL Ac<sub>2</sub>O:AcOH (1:1). The mixture was then heated up to 160°C under microwave irradiation for 0.5 h, after which the solvent was evaporated under vacuum. The crude was then purified using column chromatography (DCM:MeOH, 98:2 to 9:1) to yield compound **10** as a blue solid (144 mg, 80% yield). HPLC: *t<sub>R</sub>*: = 4.72 min; MS (*m/z*): [*M*<sup>+</sup>] calcd for C<sub>33</sub>H<sub>34</sub>N<sub>3</sub>O<sub>2</sub><sup>+</sup>: 504.3; found: 504.4; <sup>1</sup>H NMR (500 MHz, DMSO-*d*<sub>6</sub>) δ 9.26 (d, *J* = 1.3 Hz, 1H), 8.44 (s, 1H), 8.41 (s, 1H), 8.40 (d, *J* = 2.2 Hz, 1H), 8.39 (d, *J* = 2.2 Hz, 1H), 7.65 (d, *J* = 7.4 Hz, 1H), 7.56 (d, *J* = 8.0 Hz, 1H), 7.42 (dd, *J* = 8.0, 1.2 Hz, 2H), 7.40 (d, *J* = 1.1 Hz, 3H), 7.28 (ddd, *J* = 7.4, 6.5, 1.9 Hz, 2H), 5.85 (d, *J* = 14.3 Hz, 1H), 3.39 (s, 6H), 1.76 (s, 12H). <sup>13</sup>C NMR (126 MHz, DMSO) δ 177.5, 152.8, 152.4, 141.4, 139.9, 135.3, 133.7, 131.7, 131.1, 129.3, 128.8, 126.9, 126.3, 123.4, 11.9, 101.4, 52.6, 32.1, 27.5.

**4-(1,3,5,5,7,9-Hexamethyl-5*H*-4λ<sup>4</sup>,5λ<sup>4</sup>-dipyrrolo[1,2-*c*:2',1'-*f*][1,3,2]diazaborinin-10-yl)-*N*-(prop-2-yn-1-yl)benzamide (11).** 2,4-Dimethylpyrrole (4.5 mmol) and 4-carboxybenzaldehyde (2 mmol) were dissolved in DCM under Ar. One drop of TFA was added and the solution was stirred at r.t. until complete consumption of the aldehyde. Then, a solution of 2,3-dichloro-5,6-dicyano-1,4-benzoquinone (2 mmol) in DCM was added, and the stirring continued for 10 min followed by addition of triethylamine (4 mL) and BF<sub>3</sub>Et<sub>2</sub>O (4 mL). After stirring for another 2 h the reaction mixture was washed with water and dried, then solvent was evaporated under vacuum. The carboxylic acid was then purified by column chromatography (DCM: MeOH, 95:5). The crude product was then concentrated and precipitated (AcOEt: hexane, 1:1) to yield a dark red oil (160 mg, 20 % yield). HPLC: *t<sub>R</sub>*: = 5.81 min; MS (*m/z*): [*M*<sup>+</sup>] calcd for C<sub>20</sub>H<sub>19</sub>BF<sub>2</sub>N<sub>2</sub>O<sub>2</sub>: 368.2; found: 368.2. Then, the carboxylic acid (0.19 mmol) was dissolved with oxyma (0.57 mmol) in DCM and stirred for 5 min. DIC (1.14 mmol) was added and stirred for another 2 min. Propargylamine (0.21 mmol) was then added and whole mixture was stirred at r.t. for 3 h. Compound **11** was isolated as

a bright orange solid (17 mg, 22% yield over all steps). HPLC:  $t_R$ : = 5.80 min; MS ( $m/z$ ):  $[M+H]^+$  calcd for  $C_{23}H_{22}BF_2N_3O$ : 406.2; found: 406.2;  $^1H$  NMR (500 MHz,  $DMSO-d_6$ )  $\delta$  8.05 (d,  $J$  = 8.4 Hz, 2H), 7.52 (d,  $J$  = 8.4 Hz, 2H), 6.20 (s, 2H), 5.76 (s, 1H), 4.09 (dd,  $J$  = 5.6, 2.5 Hz, 2H), 2.47 (s, 6H), 1.35 (s, 6H);  $^{13}C$  NMR (126 MHz,  $DMSO$ )  $\delta$  165.7, 143.2, 135.8, 134.8, 130.9, 128.7, 122.0, 112.1, 111.6, 98.8, 73.4, 29.1, 14.7, 14.6.

**3-Oxo-6-(prop-2-yn-1-ylcarbamoyl)-3*H*-spiro[isobenzofuran-1,9'-xanthene]-3',6'-diyl**

**diacetate (12).** 5,6-carboxyfluorescein diacetate (0.43 mmol) and oxyma (1.29 mmol) were dissolved in DCM and stirred for 5 min. Then DIC (2.58 mmol) was added to the mixture, stirred for 2 min and propargylamine (1.29 mmol) was added. The whole mixture was stirred at r.t. for 3 h then evaporated under vacuum. Compound **12** was purified by column chromatography (DCM: MeOH: AcOH, 98:1:1) to yield a yellow oil (175 mg, 82% yield); HPLC:  $t_R$ : = 5.36 min; MS ( $m/z$ ):  $[M+H]^+$  calcd for  $C_{28}H_{19}NO_8$ : 497.1; found: 497.8;  $^1H$  NMR (500 MHz,  $DMSO-d_6$ )  $\delta$  9.31 (t,  $J$  = 5.5 Hz, 1H), 9.13 (t,  $J$  = 5.5 Hz, 1H), 8.54 (dd,  $J$  = 1.6, 0.7 Hz, 1H), 8.29 (dd,  $J$  = 8.1, 1.6 Hz, 1H), 8.22 (d,  $J$  = 1.4 Hz, 1H), 8.16 (dd,  $J$  = 8.1, 0.7 Hz, 1H), 7.83 (t,  $J$  = 1.0 Hz, 1H), 7.55 (dd,  $J$  = 8.0, 0.7 Hz, 1H), 7.37 – 7.28 (m, 2H), 7.02 – 6.90 (m, 6H), 4.12 (dd,  $J$  = 5.5, 2.5 Hz, 2H), 4.00 (dd,  $J$  = 5.5, 2.5 Hz, 2H), 3.16 (t,  $J$  = 2.5 Hz, 1H), 3.08 (t,  $J$  = 2.5 Hz, 1H), 2.29 (s, 3H), 2.29 (s, 3H).  $^{13}C$  NMR (126 MHz,  $DMSO$ )  $\delta$  170.3, 169.0, 167.4, 155.5, 152.4, 150.8, 135.5, 134.9, 130.0, 129.4, 119.1, 115.9, 110.6, 82.4, 81.4, 73.5, 29.6, 20.9.

**Solid-phase peptide synthesis.** All peptides were manually synthesized in polystyrene syringes fitted with a polyethylene porous disc using Fmoc-based SPPS. Solvents and soluble reagents were removed by suction. The Fmoc group was removed with piperidine: DMF (1:4) (1  $\times$  1 min, 2  $\times$  10 min). Peptide synthesis transformations and washings were performed at r.t. For peptide elongation, after the Fmoc group was removed, resins were washed with DMF (4  $\times$  1 min), DCM

(3 × 1 min) and DMF (4 × 1 min). Unless otherwise noted, standard coupling procedures were used with DIC (3 eq.) and OxymaPure (3 eq.) in DMF for 1-2 h and 5-min of pre-activation. The completion of the coupling was monitored by the Kaiser test.<sup>33</sup> Then, resins were filtered and washed with DCM (4 × 1 min) and DMF (4 × 1 min).

**Synthesis of the peptides PAF26-1/10.** For conjugates **PAF26-1**, **PAF26-2**, **PAF26-5**, **PAF26-6**, **PAF26-8**, **PAF26-9**, **PAF26-10**, standard amide bond formation coupling conditions with fluorophore-COOH (3 eq.), DIC (3 eq.) and OxymaPure (3 eq.) in DMF were used. For compounds **PAF26-3**, **PAF26-4** and **PAF26-7**, coupling of the dyes was accomplished by incubation of the peptide with the fluorophore (3 eq.) and DIPEA (3 eq.) in DMF. All resins were then washed with DMF (4 × 1 min) and DCM (3 × 1 min). For the cleavages, resins were stirred in 5 mL of TFA: H<sub>2</sub>O (95:5) for 2 h at r.t. as previously reported.<sup>34</sup> The beads were washed with TFA thoroughly and the peptides precipitated with ice-cold Et<sub>2</sub>O after rotary evaporation before final purification by semi-preparative HPLC. Characterization details can be found in the ESI.

**Synthesis of the peptides PAF26-11/12.** Azido-derivatized peptides were cleaved from the resin by cleavage with 5 mL of TFA: H<sub>2</sub>O: TIS (95:2.5:2.5) for 2 h at r.t. The beads were washed with TFA thoroughly and the peptides precipitated with ice-cold Et<sub>2</sub>O after rotary evaporation. For the conjugation was performed, the peptide (1 eq.), ascorbic acid (1 eq.), tris[(1-benzyl-1*H*-1,2,3-triazol-4-yl)methyl] amine (TBTA) (0.3 eq.) and CuSO<sub>4</sub> (0.3 eq.) were dissolved in H<sub>2</sub>O, and the corresponding alkynes (2 eq.) were added using a minimum amount of MeOH, leaving the reaction for aprox. 4 h at r.t. The reaction was monitored with HPLC, and upon completion, peptides were purified by semi-preparative HPLC. Characterization details can be found in the ESI.

**Measurement of spectral properties.** Spectroscopic data were recorded on a Synergy HT spectrophotometer (Biotek). Compounds were dissolved at concentrations around 10  $\mu$ M-50  $\mu$ M in phosphate buffer saline (PBS) and spectra were recorded at r.t.

**Culturing of *N. crassa* and *A. fumigatus*.** Cultures of *N. crassa* (wild type strain # 2489 from the Fungal Genetics Stock Center) and *A. fumigatus* (CEA10 strain from the fungal stock collection of the Manchester Fungal Infection Group) were grown on solid 100% Vogel's agar medium<sup>35</sup> at 25 °C for 3-5 days under constant light (*N. crassa*) or 37 °C for 4-5 days (*A. fumigatus*). The spores (conidia) were then harvested from the plates with sterile deionized water (*N. crassa*) or 0.05% Tween 80 in sterile deionized water (*A. fumigatus*), and the spore density was determined with a haemocytometer.

**Antifungal activity measurements.** The BacTiter-Glo™ Microbial Cell Viability Assay kit (Promega), with CELLSTAR white polystyrene flat bottomed 96-well plates (Greiner), were used for these assays. Each antifungal peptide, at an appropriate serial diluted concentrations, was mixed with conidia of *N. crassa* or *A. fumigatus* to reach a final volume of 100  $\mu$ L per well and a final conidial concentration of  $5 \times 10^5$  cells/mL in 10% liquid Vogel's medium. After 24 h of incubation (at 25 °C for *N. crassa* or 37 °C for *A. fumigatus*), the amount of fungal growth was determined by measurement of the luminescence in a TriStar LB 941 multimode microplate reader. IC<sub>50</sub> values were determined using four parameter logistic regression. Data analysis was performed using Sigma Plot 10.0. Values are represented as means  $\pm$  s.e.m. from two independent experiments ( $n = 3$ ).

**Confocal live cell microscopy.** Conidia at a concentration of  $5 \times 10^5$  cells/mL were dispensed into the wells of an 8-well slide culture chamber (ibidi USA Inc., Madison, WI) and incubated for 3 h at 25 °C (*N. crassa*) or for 16 h at 37 °C (*A. fumigatus*) in 10% Vogel's medium in order to allow



germination to occur before the addition of antifungal peptide. The peptide was added to produce the appropriate final concentration immediately before the live-cell imaging was initiated. Individual germinated spores of each species were imaged for periods of up to 1 h at the same temperature as they had previously been incubated at in a temperature-controlled chamber mounted on the microscope stage. The live-cell imaging was performed with a Leica TCS SP8 confocal laser scanning microscope equipped with photomultiplier tubes, hybrid GaAsP detectors and a 63× water immersion objective and. White light (450-750 nm), argon ion (458 nm, 476 nm, 488 nm and 496 nm) and blue diode lasers (405 nm) were used for excitation. Images were processed and analyzed using Imaris 3D/4D image processing and analysis software v 8.0 (Bitplane, Zurich, Switzerland). Details on the excitation and emission wavelengths used for all of the **PAF26-1/12** conjugates are shown in Table S2 in the ESI.

**In vivo fluorescence imaging.** Animal experiments were carried out in compliance with national and European regulations and were approved by the animal ethics committee of KU Leuven (p103-2012). 9-week-old female Balb/C mice of (Balb/cAnNCrl from Charles River Laboratories, bred at the KU Leuven animal facility, Leuven, Belgium) were kept in individually ventilated cages with free access to food and water. Immune competent mice (n = 3) were infected by inhalation of a fungal yeast cell suspension (*C. gattii* R265, 50,000 CFUs in 20 µL PBS, 10 µL per nostril) under transient isoflurane gas anesthesia (2 % in pure O<sub>2</sub>). Three weeks after infection, whole-body fluorescence imaging was carried out under isoflurane anesthesia on an IVIS Spectrum system with Living Image software (version 4.5.2, Perkin Elmer). The fluorescence signal intensity was measured using the excitation/emission 640/680 filter pair before and 5 min after intratracheal administration of 7.5 nmol of the **PAF26-10** derivative.

**Supporting Information.** NMR spectra and additional characterization data for the fluorescent PAF26 conjugates, additional imaging data. This material is available free of charge via the Internet at <http://pubs.acs.org>.

### **Author Information**

The manuscript was written with contributions of all authors. All authors have given approval to the final version of the manuscript.

\* Corresponding authors: [nick.read@manchester.ac.uk](mailto:nick.read@manchester.ac.uk); [marc.vendrell@ed.ac.uk](mailto:marc.vendrell@ed.ac.uk)

### **Acknowledgements**

A.F. acknowledges funding from the Foundation Alfonso Martin Escudero (FAME, Spain). G.V.V. acknowledges a postdoctoral fellowship of the Flemish Research Foundation (FWO). N.D.R. acknowledges funding from the Scottish Universities Life Sciences Alliance (SULSA). M.V. acknowledges funding from the Medical Research Council and the Marie Curie Career Integration Grant (333487).

### **Abbreviations**

PAF26, Peptide Antifungal 26; NBD-Cl, 4-chloro-7-nitro-2,1,3-benzoxadiazole; BODIPY, 4,4-difluoro-4-bora-3a,4a-diaza-s-indacene; TFA, trifluoroacetic acid; DIC, diisopropylcarbodiimide; DCM, dichloromethane, TBTA, tris(benzyltriazolylmethyl)amine.

## References

- [1] González-Vera, J.A. Probing the kinome in real time with fluorescent peptides. *Chem. Soc. Rev.* **2012**, *41*, 1652-1664.
- [2] Mania, D.; Hilpert, K.; Ruden, S.; Fischer, R.; Takeshita, N. Screening for antifungal peptides and their modes of action in *Aspergillus nidulans*. *Appl. Environ. Microbiol.* **2010**, *76*, 7102-7108.
- [3] Maurya, I.K.; Pathak, S.; Sharma, M.; Sanwal, H.; Chaudhary, P.; Tupe, S.; Deshpande, M.; Chauhan, V.S.; Prasad, R. Antifungal activity of novel synthetic peptides by accumulation of reactive oxygen species and disruption of cell wall against *Candida albicans*. *Peptides* **2011**, *32*, 1732-1740.
- [4] Muñoz, A.; Marcos, J.F.; Read, N.D. Concentration-dependent mechanisms of cell penetration and killing by the *de novo*-designed antifungal hexapeptide PAF26. *Mol. Microbiol.* **2012**, *8*, 89-106.
- [5] Mendive-Tapia, L.; Zhao, C.; Akram, A.R.; Preciado, S.; Albericio, F.; Lee, M.; Serrels, A.; Kielland, N.; Read, N.D.; Lavilla, R.; Vendrell, M. Spacer-free BODIPY fluorogens in antimicrobial peptides for direct imaging of fungal infection in human tissue. *Nat. Commun.* **2016**, *7*, 10940 (DOI: 10.1038/ncomms10940).
- [6] Lopez-Garcia, B.; Perez-Paya, E.; Marcos, J. F. Identification of novel hexapeptides bioactive against phytopathogenic fungi through screening of a synthetic peptide combinatorial library. *Appl. Environ. Microbiol.* **2002**, *68*, 2453–2460.

- [7] Muñoz, A.; Gandía, M.; Harries, E.; Carmona, L.; Read, N.D.; Marcos, J.F. Understanding the mechanism of action of cell penetrating antifungal peptides using the rationally designed hexapeptide PAF26 as a model. *Fungal Biol. Rev.* **2013**, *26*, 146-155.
- [8] Sudheendra, U.S.; Dhople, V.; Datta, A.; Kar, R.K.; Shelburne, C.E.; Bhunia, A.; Ramamoorthy, A. Membrane disruptive antimicrobial activities of human b-defensin-3 analogs. *Eur. J. Med. Chem.* **2015**, *91*, 91-99.
- [9] Torcato, I.M.; Huan, Y.H.; Franquelim, H.G.; Gaspar, D.; Craik, D.J.; Castanho, M.A.; Troeira Henriques, S. Design and characterization of novel antimicrobial peptides, R-BP100 and RW-BP100, with activity against Gram-negative and Gram-positive bacteria. *Biochim. Biophys. Acta* **2013**, *1828*, 944-955.
- [10] Gee, M.L.; Burton, M.; Grevis-James, A.; Hossain, M.A.; McArthur, S.; Palombo, E.A.; Wade, J.D.; Clayton, A.H. Imaging the action of antimicrobial peptides on living bacterial cells. *Sci. Rep.* **2013**, *3*, 1557.
- [11] Scheinpflug, K.; Krylova, O.; Nikolenko, H.; Thurm, C.; Dathe, M. Evidence for a novel mechanism of antimicrobial action of a cyclic R-, W-rich hexapeptide. *PLoS One* **2015**, *10*, e0125056.
- [12] Welling, M.M.; Bunschoten, A.; Kuil, J.; Nelissen, R.G.H.H.; Beekman, F.J.; Buckle, T.; van Leeuwen, F.W.B. Development of a hybrid tracer for SPECT and optical imaging of bacterial infections. *Bioconjugate Chem.* **2015**, *26*, 839–849.
- [13] Akram, A.R.; Avlonitis, N.; Lilienkamp, A.; Perez-Lopez, A.M.; McDonald, N.; Chankeshwara, S.V.; Scholefield, E.; Haslett, C.; Bradley, M.; Dhaliwal, K. A labelled-ubiquicidin

antimicrobial peptide for immediate in situ optical detection of live bacteria in human alveolar lung tissue. *Chem. Sci.* **2015**, *6*, 6971–6979.

[14] Stockert, J.C.; Abasolo, M.I.; Blazquez-Castro, A.; Horobin, R.W.; Revilla, M.; Lombardo, D.M. Selective labelling of lipid droplets in aldehyde fixed cell monolayers by lipophilic fluorochromes. *Biotech. Histochem.* **2010**, *85*, 277-283.

[15] Lee, J.S.; Vendrell, M.; Chang, Y.T. Diversity-oriented optical imaging probe development. *Curr. Opin. Chem. Biol.* **2011**, *15*, 760-767.

[16] Baker, J.G.; Middleton, R.; Adams, L.; May, L.T.; Briddon, S.J.; Kellam, B.; Hill, S.J. Influence of fluorophore and linker composition on the pharmacology of fluorescent adenosine A1 ligands. *Br. J. Pharmacol.* **2010**, *159*, 772-786.

[17] Vendrell, M.; Angulo, E.; Casadó, V.; Lluís, C.; Franco, R.; Albericio, F.; Royo, M. Novel ergopeptides as dual ligands for adenosine and dopamine receptors. *J. Med. Chem.* **2007**, *50*, 3062-3069.

[18] Davis, R.H.; Perkins, D.D. Neurospora: a model of model microbes. *Nat. Rev. Genet.* **2002**, *3*, 397–403.

[19] Brown, G.D.; Denning, D.W.; Gow, N.A.; Levitz, S.M.; Netea, M.G.; White, T.C. Hidden killers: fungal human infections. *Sci. Transl. Med.* **2012**, *19*, 4, 165rv13.

[20] Jansenn, M.J.; Ensing, K.; de Zeeuw, R.A. Fluorescent-labeled ligands for the benzodiazepine receptor. Part 2: The choice of an optimal fluorescent-labeled ligand for benzodiazepine receptor assays. *Pharmazie* **2000**, *55*, 102-106.

- [21] Lee, J.S.; Kang, N.Y.; Kim, Y.K.; Kim, H.K.; Samanta, A.; Feng, S.; Vendrell, M.; Park, J.H.; Chang, Y.T. Synthesis of a BODIPY library and its application to the development of live cell glucagon imaging probe. *J. Am. Chem. Soc.* **2009**, *131*, 10077-10082.
- [22] Samanta, A.; Vendrell, M.; Das, R.; Chang, Y.T. Development of photostable near-infrared cyanine dyes. *Chem. Commun.* **2010**, *46*, 7406-7408.
- [23] Zhai, D.; Lee, S.C.; Vendrell, M.; Leong, L.P.; Chang, Y.T. Synthesis of a novel BODIPY library and its application in the discovery of a fructose sensor. *ACS Comb. Sci.* **2012**, *14*, 81-84.
- [24] Er, J.C.; Vendrell, M.; Tang, M.K.; Zhai, D.; Chang, Y.T. Fluorescent dye cocktail for multiplex drug-site mapping on human serum albumin. *ACS Comb. Sci.* **2013**, *15*, 452-457.
- [25] Rimpelova, S.; Briza, T.; Kralova, J.; Zaruba, K.; Kejik, Z.; Cisarova, I.; Martasek, P.; Ruml, T.; Kral, V. Rational design of chemical ligands for selective mitochondrial targeting. *Bioconjugate Chem.* **2013**, *24*, 1445-1454.
- [26] Tajalli, H.; Gilani, A.G.; Zaherhamidi, M.S.; Tajalli, P. The photophysical properties of Nile red and Nile blue in ordered anisotropic media. *Dyes Pigments* **2008**, *78*, 15-24.
- [27] Loving, G.S.; Sainlos, M.; Imperiali, B. Monitoring protein interactions and dynamics with solvatochromic fluorophores. *Trends Biotechnol.* **2010**, *28*, 73-83.
- [28] Frangioni, J.V. In vivo near-infrared fluorescence imaging. *Curr. Opin. Chem. Biol.* **2003**, *7*, 626-634.
- [29] Vendrell, M.; Samanta, A.; Yun, S.W.; Chang, Y.T. Synthesis and characterization of a cell-permeable near-infrared fluorescent deoxyglucose analogue for cancer cell imaging. *Org. Biomol. Chem.* **2011**, *9*, 4760-4762.

- [30] Samanta, A., Vendrell, M., Yun, S.W., Guan, Z., Xu, Q.H., Chang, Y.T. A photostable near-IR protein labeling dye for in vivo imaging. *Chem. Asian J.* **2011**, 6, 1353-1357.
- [31] Xin, J., Zhang, X., Liang, J., Xia, L., Yin, J., Nie, Y., Wu, K., Tian, J. In vivo gastric cancer targeting and imaging using novel symmetric cyanine dye-conjugated GX1 peptide probes. *Bioconjugate Chem.* **2013**, 24, 1134-1143.
- [32] Kim, E.M., Park, E.H., Cheong, S.J., Lee, C.M., Jeong, H.J., Kim, D.W., Lim, S.T., Sohn, M.H. In vivo imaging of mesenchymal-epithelial transition factor (c-Met) expression using an optical imaging system. *Bioconjugate Chem.* **2009**, 20, 1299-1306.
- [33] Kaiser, E., Colecott, R. L., Bossinger C. D., Cook, P. I. Color test for detection of free terminal amino groups in the solid-phase synthesis of peptides. *Anal. Biochem.* **1970**, 34, 595-598.
- [34] Yraola, F.; Ventura, R.; Vendrell, M.; Colombo, A.; Fernández, J. C.; de la Figuera, N.; Fernández-Forner, D.; Royo, M.; Forns, P.; Albericio, F. A re-evaluation on the use of Rink, BAL and PAL resins and linkers. *QSAR Comb. Sci.* **2004**, 23, 145-152.
- [35] Vogel, H. J. A convenient growth medium for Neurospora (Medium N). *Microbial Genet. Bull.* **1956**, 13, 42-43.

## Table of Contents Graphic

**Not just a pretty color.** The synthesis and systematic evaluation of a library of fluorescent antimicrobial sequences provides new insights on the fluorophores of choice for different bioimaging applications.

